Structural and Multidisciplinary Optimization (2025) 68:128
https://doi.org/10.1007/s00158-025-04041-8

RESEARCH PAPER

Optimum local reinforcements for maximum strength of composite plates with a cutout

Sinan Kaya[1] · **Fazil O. Sonmez**[1]

Received: 7 July 2024 / Revised: 3 March 2025 / Accepted: 15 May 2025 / Published online: 15 July 2025
© The Author(s) 2025

Abstract
This study aims to find the optimum design of reinforcing layers placed around the hole in a composite laminated plate to maximize its first-ply and ultimate failure strengths with minimum use of reinforcing material. The ultimate failure load is determined using a progressive damage model incorporating the Puck failure criterion and the material property degradation method. A finite element model is developed to simulate the structural response under loading. The model's accuracy is confirmed by comparing its predictions with existing experimental data. The optimum local reinforcement designs are identified using a modified simulated annealing algorithm, which is made more reliable and easier to apply with the improvements introduced in this study. The optimization variables are chosen as the fiber orientation angles and the dimensions of the reinforcing layers. Optimizations are performed for different configurations of local reinforcements to determine the most effective way of placing the reinforcing layers. Significant improvements in the strength are obtained with minimal added mass through optimization.

Keywords Laminated composites · Notches · First-ply failure strength · Ultimate strength · Progressive damage analysis · FEA · Modified simulated annealing

1 Introduction

Thin-walled shell structures made of continuous fiber-reinforced composite materials are vital components of aircraft, spacecraft, and automotive vehicles owing to their lightweight, high strength, superior corrosion resistance, and tailorable material properties. These structural elements mostly contain cutouts that act as doorways, windows, access ports, or as a way to reduce weight. A composite structure is gravely weakened if a cutout is needed for functional purposes. These structures are required to be damage tolerant, meaning they should continue to support design loads even in case damage occurs. Increasing the thickness all the way through the structure is an inefficient way of strengthening the structure, considering that this results in considerable material cost and increased weight. Instead, making the weaker regions stronger, for example, applying local reinforcements around the notches and in the regions where high stresses develop is a much more effective way of making the whole structure stronger. By locally reinforcing a structure, one may reduce local deformations and stress concentrations around the cutouts so as to prevent premature failures or local buckling. To do this, first, one must be able to estimate how a cutout affects the structural response of a composite part and how a reinforcement changes the stress distribution. The structural response can be predicted using a reliable structural analysis method. Secondly, one should be able to estimate how a reinforcement around a cutout affects the load-carrying capacity of a composite structure. This requires a reliable failure analysis method. Thirdly, one should be able to find effective reinforcement designs to improve the structural performance. This can be accomplished by employing an effective optimization algorithm, which can determine the optimum size, shape, and location of the reinforcements.

The failure behavior of glass or carbon-fiber-reinforced plastics is predominantly brittle. As a result, they are liable to fail catastrophically. Designing composite structures by just considering the first-ply failure load may lead to safe designs

Responsible Editor: Axel Schumacher.

✉ Fazil O. Sonmez
sonmezfa@bogazici.edu.tr

[1] Department of Mechanical Engineering, Bogazici University, Istanbul, Bebek 34342, Turkey

for normally expected loads. However, a catastrophic failure that may occur due to an unexpected overload is unacceptable. A composite structure should maintain its structural integrity in case of damage. The structures should exhibit considerable damage tolerance and residual strength after initial damage. Relying solely on first-ply failure criteria may lead to unsafe designs. In order to ensure the safety of a structure, one should consider its ultimate load-carrying capacity in the design. For this purpose, progressive failure analysis (PFA) techniques are used. PFA allows one to predict the damage progression in the composite material as the load is increased, ultimately leading to a breakdown of the structure's ability to sustain any load.

Researchers mainly used two approaches to determine the damage progression until the final failure: One is ply-discounting (Spottswood and Palazotto 2001; Kweon 1998; Gummadi and Palazotto 1998; Gotsis et al. 1998, 2004; Xie and Biggers 2003; Ambur, et al. 2004; Ambur, et al. 2004; Prusty 2005; Irvine and Ginty 1986; Riccio et al. 2017), which is setting the values of some elastic properties of the damaged plies to zero or assigning a negligibly small value, such as transverse modulus, E_{22}, in-plane shear modulus, G_{12}. The other (Riccio et al. 2017; Camanho and Matthews 1999; Kim et al. 1996; Tan 1991; Chang and Chang 1987; O'Higgins et al. 2004; McCarthy et al. 2005; Günel and Kayran 2013; Philippidis and Antoniou 2013; Basu et al. 2007; Hinton et al. 2004; Liu and Tsai 1998; Goyal et al. 2004) is to degrade the stiffness properties by multiplying with predefined factors having values between 0.0 and 1.0 when damage is predicted, considering that the failed plies retain some residual strength. Suitable values for these factors are usually found by trial and error (Tan 1991; Chang and Chang 1987; O'Higgins et al. 2004; McCarthy et al. 2005; Günel and Kayran 2013; Philippidis and Antoniou 2013; Liu and Tsai 1998), using experimental data (Kim et al. 1996; Basu et al. 2007), or using a continuum damage model (McCarthy et al. 2005). These degradation factors are either constant (Ambur, et al. 2004; Ambur, et al. 2004; Camanho and Matthews 1999; McCarthy et al. 2005; Liu and Tsai 1998; Goyal et al. 2004) or dependent on the level of stress or failure index (Chang and Chang 1987; Günel and Kayran 2013; Philippidis and Antoniou 2013; Goyal et al. 2004).

In the studies where a progressive failure analysis method is proposed, the researchers considered unnotched laminated plates (Gotsis et al. 2004; Prusty 2005; Philippidis and Antoniou 2013), plates with a circular open-hole (Irvine and Ginty 1986; Riccio et al. 2017; Kim et al. 1996; Tan 1991; Chang and Chang 1987; O'Higgins et al. 2004; Günel and Kayran 2013; Basu et al. 2007; Goyal et al. 2004; Zhang and Zhao 2012; Moure et al. 2015; Lee et al. 2015; Maimí et al. 2007a; Maimí et al. 2007b; Ridha et al. 2014; Din et al. 2018; Chen et al. 2012; Hallett et al. 2009; Zhou et al. 2017; Soutis et al. 1991; Su et al. 2015), with a slit (Irvine and Ginty 1986; Riccio et al. 2017), repaired laminated plates (Liu and Wang 2007), bolted joints (Camanho and Matthews 1999; McCarthy et al. 2005), stiffened plates (Ambur et al. 2004; Prusty 2005; Riccio et al. 2017; Ridha et al. 2014; Kong et al. 1998), cylindrical shells (Kweon 1998; Gummadi and Palazotto 1998; Xie and Biggers 2003), and curved panels with a circular cutout (Xie and Biggers 2003; Ambur, et al. 2004).

The researchers conducting progressive failure analysis of composite structures considered mostly uniaxial in-plane tension (Irvine and Ginty 1986; Kim et al. 1996; Tan 1991; O'Higgins et al. 2004; Günel and Kayran 2013; Philippidis and Antoniou 2013; Ridha et al. 2014; Hallett et al. 2009) and also in-plane compression (Kweon 1998; Ambur, et al. 2004; Philippidis and Antoniou 2013; Basu et al. 2007; Goyal et al. 2004; Zhou et al. 2017; Soutis et al. 1991; Su et al. 2015; Tan and Perez 1993), torsion (Gummadi and Palazotto 1998), biaxial loading (Gotsis et al. 2004; Liu and Tsai 1998), shear loading (Ambur et al. 2004; Goyal et al. 2004), in-plane compression applied on laminates after being impact damaged (Shroff and Kassapoglou 2015), and out-of-plane loading (Günel and Kayran 2013; Padhi et al. 1997).

In order to predict damage, first, a structural analysis should be carried out. For this purpose, the researchers used the finite element method. The location and the type of damage the structure sustains were predicted using a failure criterion like Tsai-Wu (Prusty 2005; Zhou et al. 2017; Liu and Wang 2007; Kong et al. 1998), Hashin (Gummadi and Palazotto 1998; Ambur et al. 2004; Camanho and Matthews 1999; O'Higgins et al. 2004; McCarthy et al. 2005; Goyal et al. 2004; Chen et al. 2012), the modified Hashin (Xie and Biggers 2003), Puck (Lee et al. 2015; Din et al. 2018; Deuschle and Puck 2013), and Larc04 (Maimí et al. 2007b) criteria.

Being tailorable, composite materials are amenable to modification of their material system in many different ways for improved structural performance for different applications. As design variables, not only their shape and size but also the number of layers, the fiber orientation and thickness of each layer, and the material of the layers can be changed to obtain the most effective use of the material for a specific application. With a high number of variables, finding the optimum combination for these variables promises a significant gain but also poses difficulty. For this reason, design optimization of composites drew the attention of many researchers (Nikbakt et al. 2018; Sonmez 2017). Among them, some studies focused on the optimum design of notched composite constructions to maximize the strength (Le-Manh and Lee 2014; Catapano et al. 2015; Huang and Haftka 2005; Almeida Jr et al. 2020; Tanaka et al. 2021; Ferreira and Ashcroft 2020).

Although significant gain can be obtained in strength by locally reinforcing notched composite structures, quite a few studies in the literature considered this problem. Schlapfer and Kress (Schläpfer and Kress 2014) proposed a strength improvement method to determine the optimum local reinforcements placed around the hole of a composite laminate. In that method, sensitivities for layer thickness changes were calculated for each finite element. Local reinforcements were introduced by assigning thickness values to initially zero-thickness virtual layers based on the sensitivity information. The increase achieved in the first-ply failure strength using the optimum local reinforcement was 100% with only 6% additional reinforcement material. Huang and Haftka (Huang and Haftka 2005) employed the finite element method (FEM) to optimize the fiber orientation of each element around a circular hole. The main goal of that study was to identify the most suitable fiber orientations that would maximize the load-carrying capacity of the structure based on the Tsai-Wu failure criterion. The optimization results showed the effectiveness of this approach in improving the strength of notched composite plates. Similar studies (Arian Nik et al. 2022; Matsuzaki et al. 2021; Izzi et al. 2021; Khani et al. 2017; Huang et al. 2016) were also conducted; however, the main drawback of this method is the difficulty in manufacturing a laminate composed of layers with variable fiber orientations. Matias et al. (Mathias et al. 2006) used a genetic algorithm to reduce the stress concentration in a metal plate by optimizing the shape, location, and fiber orientations of a composite patch bonded onto the plate.

One way of locally reinforcing a notched laminate is using additional layers around the notch. Figure 1 shows some reinforcement configurations that may improve the load-carrying capacity of plates with a hole. By determining the optimal size and layup sequence of these additional layers and their optimal placement, one can significantly improve the laminate strength with a slight increase in the material used. The goal of this study is to determine the optimal local reinforcement designs that maximize the first and final failure loads of composite laminates having a hole with minimum use of reinforcing material.

In the previous studies, the optimum designs are identified based on the first-ply failure load. This means the load causing initial damage was maximized with no regard to the ultimate failure load. In this study, the optimum designs are identified based on the ultimate strength. The failure load causing initial damage at locally high-stressed regions around a cutout is usually a small fraction of the ultimate failure load of the composite structure. The experimental studies on the failure behavior of open-hole tension specimens, like references (Tan 1991; O'Higgins et al. 2004; Joseph, et al. 2015), show that the overall stiffness of the specimens degrades only after considerable accumulation of damage. This means that small-scale local damage can be tolerated under working loads for notched composite structures. The design of notched composite structures should be based on the full knowledge of damage tolerance and the final strength. For this reason, maximum-strength design of notched composites should be based on not only the first-ply failure strength but also the final failure strength. In this study, a multi-objective design optimization procedure is proposed that improves both the first and final failure loads.

The previous studies that introduced design optimization methods to maximize the strength of notched composite laminates by locally reinforcing them, used the variable-thickness or variable fiber orientation approach (Huang and Haftka 2005; Mathias et al. 2006; Zehnder and Ermanni 2006; Lopes et al. 2010; Hyer and Lee 1991; Khani et al. 2011). Although promising results were obtained in those studies, their application requires automated tow-placement machines, which impedes widespread industrial application of those methods. In this study, considering the manufacturability of the optimum designs, additional rectangular layers around the cutout are used as reinforcing elements.

Structural optimization problems have numerous locally optimal designs, which makes it necessary to use a global search algorithm to find the best design. For this purpose, a

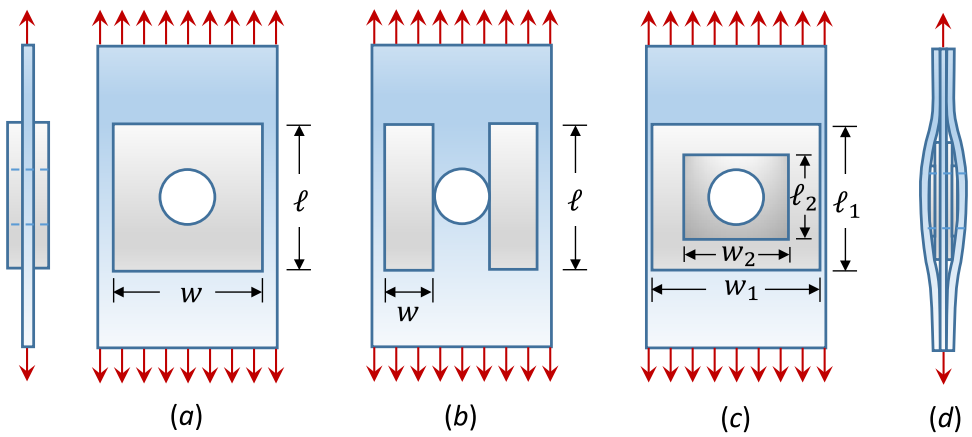

Fig. 1 Possible local reinforcement configurations

previously (Kayikci and Sonmez 2012; Akbulut and Sonmez 2011) proposed modified simulated annealing algorithm is used. As a novel contribution of the present study, several additional improvements are introduced to enhance its reliability and ease of applicability. While the parameters of the classical simulated annealing algorithm need to be tuned for the type of the optimization problem; in the modified simulated annealing algorithm, the users need to specify only the upper and lower limits of the optimization variables, and the algorithm tunes itself to the specific problem at hand.

Considering that design optimization requires many iterations, a progressive failure analysis method is computationally too expensive for typical industrial applications. As a way to overcome this difficulty, the applicability of design optimization based on a first-fiber failure approach in maximizing the final failure load is also investigated in this study.

Very promising results are obtained using the approach proposed in this study. With the optimum use of reinforcements, the final failure load improves by more than 130% compared to an unreinforced plate, with a maximum weight increase of just 16%. Besides, the first-ply failure load doubles. This study underscores the effectiveness of local reinforcements in areas of stress concentration, significantly enhancing both initial and ultimate failure loads while minimizing reinforcement needs without compromising manufacturing feasibility.

2 The methodology for the progressive failure analysis of composite laminates

First, a finite element model of the composite plate with a circular hole is developed to obtain its structural response under increasing load with progressing damage. In tension or compression tests of composite specimens, the usual practice is to apply displacement-controlled load. The boundary conditions in the FE model are chosen to reflect the actual test loading conditions. The nodes of one edge of the plate are fixed, and a certain displacement is defined for the nodes of the other edge. Then, the resulting deformation and stress distribution are determined. Using the Puck failure criterion, the failure index of the material for all plies in each finite element is calculated based on the stress state in the element. If the failure index reaches 1.0 at a layer in an element, which means the material at that layer has failed in a specific failure mode, then its stiffness is degraded using the material property degradation method. Subsequently, the applied displacement is incrementally increased in magnitude. At each step, the structural and failure analyses are repeated, and the material properties in the damaged elements are degraded. The total applied force is obtained from the reaction forces at the fixed end. Typically, the total force increases until the ultimate failure occurs, then it drops. The final value of the applied displacement is chosen so that the ultimate failure is ensured to have occurred before the final displacement is applied.

2.1 Determining the ultimate failure load

At each incremental step of increasing the displacement at the loaded edge of the plate and carrying out the damage analysis, the reaction force at the fixed edge is calculated. The load applied to the plate is taken to be the same as the total reaction force in the loading direction, and thus, the load–displacement relation is obtained. Figure 2 shows a typical load–displacement curve of an open-hole tension test specimen predicted by the present model. Small-scale damage around the hole does not cause significant degradation in the stiffness. According to the present progressive failure model, the initial damage to the matrix occurs at 21.6 kN, while the initial fiber damage occurs at 39.7 kN. Prior to fiber damage, the load—displacement diagram has constant slope, indicating negligible stiffness degradation. However, after the initial fiber damage, further fiber failures are triggered with the increase in the load, resulting in noticeable degradation in the stiffness. When the damage becomes extensive and approaches the edges of the specimen, a significant drop occurs in the load, which means the structure's resistance to further deformation suddenly decreases. The ultimate failure load is defined in this study as the peak load that the plate sustains before a significant drop occurs in the load level. After sustaining significant damage resulting in a significant drop in the load level, the part is considered incapable of functioning properly.

Recognizing that the decrease in the slope of the load–displacement curve is small up to the peak point, which means the plate maintains its stiffness to a large extent, one may assume that intralaminar damage dominates the damage behavior of the material up to the peak point rather than interlaminar damage, or delamination, since extensive delamination is known to result in considerable degradation in the stiffness (Alpay et al. 2023). After the peak point, on the other hand, one should assume that not only extensive intralaminar damage but also extensive interlaminar damage occurs. Considering that the objective of the design optimization in this study is to maximize not only the first-ply failure strength but also the ultimate strength of plates with open holes, only the intralaminar damage is accounted for using the Puck failure criteria, and delamination is neglected since accurately obtaining the post-failure behavior of the plates is not required for the solution of the problem considered in this study.

Although the load–displacement curves of the laminates considered in this study are like the one in Fig. 2, for some different layups, one or two drops may occur in the load level before the ultimate peak load is reached. In such cases,

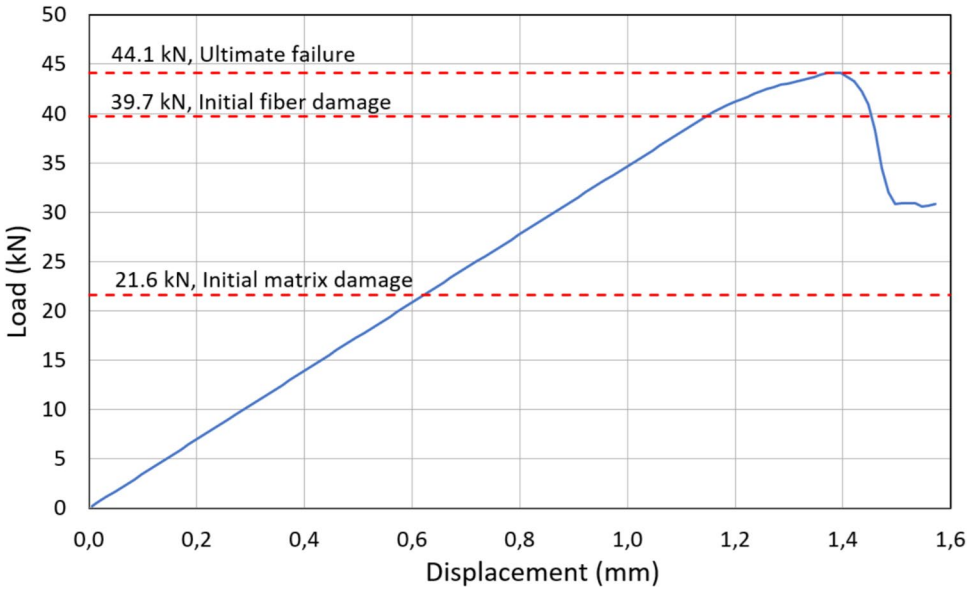

Fig. 2 The load–displacement relation predicted by the present model for the OHT1 test specimen with $[45/0/-45/90]_{2s}$ stacking sequence made of IM7-8552 material reported by Marlett (Marlett et al. 2011)

the local reinforcement should be optimized to maximize the first peak load. In this way, the first peak load can be made closer to the peak load, or interim peaks can be totally eliminated.

2.2 Puck failure criterion

Puck et al. (Puck et al. 2002; Puck and Schürmann 2004; Puck and Mannigel 2007) considered mainly two failure modes having different failure mechanisms; one is fiber failure (FF), and the other is inter-fiber fracture (IFF), or matrix cracking.

2.2.1 Fiber Failure (FF)

Fiber damage is mainly caused by stresses in the fiber direction. In the simpler version, the criterion for fiber damage follows the maximum stress criterion. Fiber failure is predicted if

$$\sigma_{11} \geq X_t \; or \; \sigma_{11} \leq X_c \tag{1}$$

where σ_{11} is the normal stress in the fiber direction and X_t and X_c are the tensile and compressive strengths of the material along the fibers, respectively. Puck proposed a more refined criterion for fiber failure considering the Poisson effect of the transverse stresses (σ_{22}, σ_{33}) on the normal strain in the fiber direction (ε_{11}) (Puck and Schürmann 2004). However, in this study, interactions between σ_{11} and the other stress components are neglected considering the predominant effect of σ_{11} on the fiber damage, and Eq. (1) is used to predict the fiber failure.

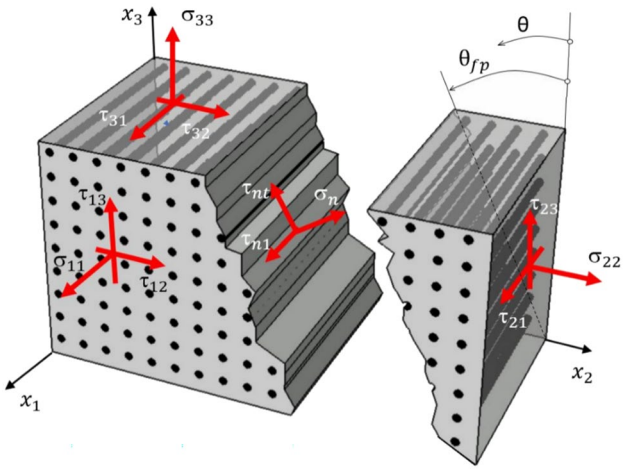

Fig. 3 Stress state, σ_n, τ_{nt},τ_{n1}, on the fracture plane, which is inclined with angle θ_{fp}

2.2.2 Inter-fiber fracture (IFF)

IFF, or matrix cracking, is defined as the development of a macroscopic crack on a plane parallel to the fibers. Considering a 3D stress state,σ_{ij}, in an element, IFF occurs in a plane inclined with angle θ_{fp} (Fig. 3). Puck observed that IFF occurred in carbon or glass-fiber/epoxy laminates in a certain fracture plane with a brittle manner without any significant plastic deformation, and following Mohr, assumed that fracture was dependent only on the stress state on the fracture plane,σ_n,τ_{nt},τ_{n1} (Fig. 3) (Puck et al. 2002; Puck and Schürmann 2004; Knops 2008). The effect of normal stress in the fiber direction,σ_{11}, on IFF is considered negligible as

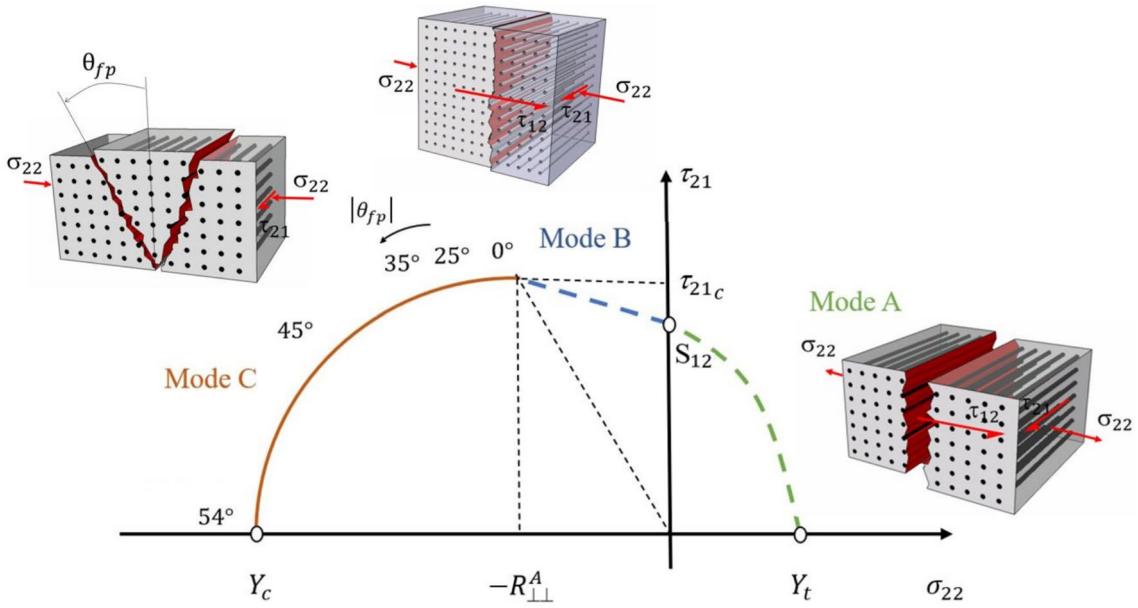

Fig. 4 Typical inter-fiber fracture (IFF) curve of continuous fiber-reinforced plastics for σ_{22} and τ_{21} stress combinations

long as it is much smaller than the corresponding strength ($\sigma_{11} \ll X_t$ and $|\sigma_{11}| \ll |X_c|$).

Because laminated composites are thin-walled structures, the typical loading state is plane stress, where only σ_{11}, σ_{22}, and τ_{21} are non-zero stress components. Using the following stress transformation rules, one can easily calculate the stresses on any transverse plane: $\sigma_n = \sigma_{22}\cos^2\theta$, $\tau_{nt} = -\sigma_{22}\sin\theta\cos\theta$, $\tau_{n1} = \tau_{21}\cos\theta$. Puck distinguished three different modes for IFF; Mode *A*, Mode *B*, and Mode *C*. Based on the following observations (Knops 2008), different stress states can be associated with one of these modes:

Mode A: Application of tensile σ_{22} and in-plane shear stress τ_{12} causes fracture at the x_2- plane, $\theta_{fp} = 0°$ (Fig. 3). If pure σ_{22} is applied, fracture occurs at $\sigma_{22} = Y_t$, the transverse strength of the material in tension. If pure τ_{21} is applied, fracture occurs at $\tau_{21} = S_{12}$, the in-plane shear strength of the material. When both σ_{22} and τ_{21} act together, they interact in a way that changes the failure threshold compared to when each stress is applied separately. Therefore, their combined effect must be taken into account when predicting material failure. As depicted in Fig. 4 (dashed green line), in the presence of τ_{21}, failure due to tension in the x_2 direction (σ_{22}) occurs at a lower value than Y_t. That means there is a strong interaction between σ_{22} and τ_{21}. IFF occurs in Mode *A* if the following inequality holds:

$$\sqrt{\left(\frac{\tau_{21}}{S_{21}}\right)^2 + \left(1 - p^{(+)}_{\perp\parallel}\frac{Y_t}{S_{12}}\right)^2\left(\frac{\sigma_{22}}{Y_t}\right)^2} + p^{(+)}_{\perp\parallel}\frac{\sigma_{22}}{S_{12}} \geq 1 \qquad \text{if } \sigma_{22} \geq 0 \tag{2}$$

The values suggested by Puck et al. (Puck et al. 2002; Puck and Schürmann 2004) for the inclination parameters are $p^{(+)}_{\perp\parallel} = 0.35$, $p^{(-)}_{\perp\parallel} = 0.3$, $p^{(-)}_{\perp\perp} = 0.25$, $p^{(+)}_{\perp\perp} = 0.25$ for carbon-fiber/epoxy materials.

Mode B: Application of moderate levels of compressive σ_{22} and in-plane shear stress τ_{21} causes fracture again at the x_2-plane, $\theta_{fp} = 0°$. Compressive normal stress hinders fracture. As seen in Fig. 4 (dashed blue line), with an increased magnitude of σ_{22} in compression, τ_{21} can be increased beyond S_{12} without incurring fracture. IFF occurs in Mode *A* if the following inequality holds:

$$\frac{1}{S_{12}}\left(\sqrt{\tau_{21}^2 + \left(p^{(-)}_{\perp\parallel}\sigma_{22}\right)^2} + p^{(-)}_{\perp\parallel}\sigma_{22}\right) \geq 1 \qquad \text{if } \sigma_{22} < 0 \text{ and } \left|\frac{\sigma_{22}}{\tau_{21}}\right| \leq \frac{R^A_{\perp\perp}}{|\tau_{21c}|} \tag{3}$$

The transition between Mode B and Mode C is dictated by the ratio $R^A_{\perp\perp}/|\tau_{21c}|$. These parameters are given by

$$R^A_{\perp\perp} = S_{12}\frac{p^{(-)}_{\perp\perp}}{p^{(-)}_{\perp\parallel}} \qquad \tau_{12c} = S_{12}\sqrt{1 + 2p^{(-)}_{\perp\perp}} \tag{4}$$

Detailed information regarding the inclination parameters,$p^{(-)}_{\perp\perp}$ and $p^{(-)}_{\perp\parallel}$, are given in reference (Knops 2008).

Mode C: Application of in-plane shear stress τ_{12} combined with a high compressive σ_{22} causes fracture at an oblique plane with $\theta_{fp} \neq 0°$ (Fig. 4). The transverse plane is no longer the fracture plane. The inclination angle, θ_{fp},

increases as the magnitude of the compressive stress, σ_{22}, is increased until it reaches about $\pm 54°$ for pure compressive stress with a magnitude equal to Y_c (see solid orange line in Fig. 4). IFF occurs in Mode C if the following inequality holds:

$$\left[\left(\frac{\tau_{21}}{2\left(1+p_{\perp\perp}^{(-)}S_{12}\right)}\right)^2+\left(\frac{\sigma_{22}}{Y_c}\right)^2\right]\frac{Y_c}{|\sigma_{22}|}\geq 1 \quad \text{if } \sigma_{22}<0 \text{ and } \left|\frac{\tau_{21}}{\sigma_{22}}\right|\leq\frac{|\tau_{21c}|}{R_{\perp\perp}^A} \tag{5}$$

3D forms of the Puck's model are given in references (Puck et al. 2002; Puck and Schürmann 2004).

2.3 Material property degradation method

Once initial material damage occurs under a given loading condition, stiffness properties in the damaged region degrade. As a result, the load is redistributed within the structure in such a manner that the undamaged regions sustain the load. Further increase in the load causes progression of damage. Prediction of the structural response after the onset of damage requires a proper degradation scheme that correctly reflects the residual stiffness of the damaged material.

In this study, the material property degradation method is adopted. In this method, stiffness properties are multiplied by degradation factors once the criterion for damage initiation is met. The undamaged material is assumed to be linearly elastic. Fiber-reinforced plastics are brittle, which means negligible plastic deformation occurs until fracture. Then, their structural response can be assumed to be linearly elastic until ultimate failure occurs.

Since composite plates are thin, structural analysis can be carried out using plane stress formulations, in which only in-plane stress components are nonzero, σ_{11}, σ_{22}, and τ_{12}. The Puck failure criterion is used to determine damage initiation in a finite element. Constitutive equations for a damaged material are expressed in the material coordinates in which fibers are oriented in the x_1 direction as follows (Lapczyk and Hurtado 2007)

$$\{\sigma\}=[C]_d\{\varepsilon\} \tag{6}$$

or

$$\begin{Bmatrix}\sigma_{11}\\ \sigma_{22}\\ \tau_{12}\end{Bmatrix}=\frac{1}{D}\begin{bmatrix}(1-d_f)E_{11} & (1-d_f)(1-d_m)\nu_{12}E_{22} & 0\\ (1-d_f)(1-d_m)\nu_{21}E_{11} & (1-d_m)E_{22} & 0\\ 0 & 0 & D(1-d_s)G_{12}\end{bmatrix}\begin{Bmatrix}\varepsilon_{11}\\ \varepsilon_{22}\\ \gamma_{12}\end{Bmatrix}, \tag{7}$$

where σ_{11}, σ_{22}, and τ_{12} are effective in-plane stress components, ε_{11}, ε_{22}, and γ_{12} are in-plane strain components, d_f and d_m are the degradation parameters for fiber failure and matrix failure, respectively; E_{11}, E_{22}, and G_{12} are moduli of the undamaged material, ν_{12} and ν_{21} are Poisson's ratios of the undamaged material; $D=1-(1-d_f)(1-d_m)\nu_{12}\nu_{21}$. Maxwell–Betti reciprocal theorem requires that $\nu_{12}/E_{11}=\nu_{21}/E_{22}$ (Barbero 2007). The theorem also holds for damaged material as in Eq. (7). The degradation parameters may have different values for damage under tension and compression, which will be denoted by superscripts "+" and "- " as $d_f^+, d_f^-, d_m^+, d_m^-$. The degradation parameter for shear is not taken as an independent parameter, and it is expressed in terms of the other parameters (Lapczyk and Hurtado 2007) as

$$d_s=1-\left(1-d_f^+\right)\left(1-d_f^-\right)\left(1-d_m^+\right)\left(1-d_m^-\right) \tag{8}$$

The degradation parameters take values between 0 and 1. A value of 0 means no damage, 1.0 means total loss of stiffness. When the failure criterion predicts matrix or fiber damage, the corresponding degradation parameter takes its full value, which means the material stiffness is assumed to decrease suddenly when damage occurs.

The degradation parameters control how the stiffness of the material degrades after the onset of damage. It is challenging to ascertain the correct values of the degradation parameters for the composite materials due to the existence of different failure modes, interaction between them, effects of various factors like the types of fibers and matrix materials, volume fraction of the fibers, interactions between layers with different fiber orientations. Researchers proposed different approaches to determine the values of the degradation parameters and suggested different values for these parameters (Garnich and Akula 2009).

Based on the correlations obtained between the numerical results of the model proposed in this study and the open-hole tension and compression test results reported in the previous studies (Marlett et al. 2011; Clarkson 2011), the following values are adopted for the degradation parameters: $d_f^+ = 0.999$, $d_f^- = 0.9$, $d_m^+ = 0.8$, $d_m^- = 0.8$. These values are within the range proposed in the previous studies on the progressive damage behavior of composite materials (Garnich and Akula 2009). According to these values, fiber breakage under tension leads to almost complete loss of the load-bearing capacity of the material under tension, while the material retains about 10% of its strength after fiber failure under compression. On the other hand, matrix failure in the form of inter-fiber fracture leads to an 80% reduction in the strength in tension or compression.

3 Validation of the progressive failure analysis

In order to validate the progressive failure analysis and the finite element model, the empirically obtained failure loads of open-hole tension specimens reported by the experimental studies are compared with the predicted ones.

3.1 Case 1

Marlett (Marlett et al. 2011) and Clarkson (Garnich and Akula 2009) from the National Center for Advanced Materials Performance (NCAMP) reported the ultimate tensile strengths of open-hole tension test specimens with two different materials and three different layup sequences:

1. Quasi-isotropic specimens were tested with $[45/0/-45/90]_{2s}$ stacking sequence, denoted as OHT1.
2. Soft specimens with $[\pm 45/0/\pm 45/90/\pm 45/\pm 45]_s$ stacking sequence were tested, in which 10% of the fibers were in the loading direction, 10% in the transverse direction, and the rest were oriented with ± 45 degrees, referred to as OHT2.
3. Hard laminates with $[0/45/0/90/0/-45/0/45/0/-45]_s$ $[0/45/0/90/0/-45/0/45/0/-45]_s$ stacking sequence were tested with 50% of the fibers in the loading direction, 10% in the transverse direction, and 40% in the ± 45-degree direction, labeled as OHT3.

Two carbon-fiber-reinforced composite materials commonly used in aerospace industry were chosen for the specimens, IM7/8552 and AS4/8852. The material properties reported by Marlett (Marlett et al. 2011) and Clarkson (2011) are given in Table 1. The tests were conducted in line with ASTM D5766 standard. According to the standard, the width of the open-hole specimens was 1.5 inches (38.1 mm), and the hole diameter was 0.25 inches (6.35 mm).

Using ANSYS commercial FEA software, a finite element model is developed to simulate the open-hole tension tests and determine the structural response of the specimens. Through the use of ANSYS Parametric Design Language (APDL), a code is developed to carry out the finite element analysis and to implement the Puck failure criteria and the material property degradation method.

SHELL181, a layered structural shell element with four nodes, is used to mesh the area (Fig. 5). Each node has six degrees of freedom, three translational degrees (u_x,u_y, u_z) and three rotational degrees (θ_x,θ_y,θ_z). The number of integration points through the thickness of each layer is chosen as three. Because progressive failure analysis is continued until the final failure occurs, displacements cannot be assumed small. For this reason, the effects of geometric nonlinearity are included by employing the Newton–Raphson method, in which the load is divided into a sequence of load increments that can be applied throughout many load steps.

In the actual tests, one end of the specimen is clamped, and the other end is loaded with displacement control. Accordingly, the nodes on one side of the FE model are fixed; the nodes on the other side are restrained from movement in all the degrees of freedom except the x-direction. A certain displacement is applied in the x-direction such that it is sufficient to cause ultimate failure. For the quasi-isotropic AS4/8552 laminate, $u_x(L) = 1.6$ mm is applied, and the ultimate failure occurs at 1.37 mm. For the soft (OHT2) and hard (OHT3) laminates, the ultimate failure occurs at 1.58 mm and 1.21 mm, respectively. A convergence analysis is conducted to ensure the accuracy

Table 1 The properties of the specimens tested by Marlett (Marlett et al. 2011) and Clarkson (2011)

Property	Material	
	IM7/8552 (Marlett et al. 2011)	AS4/8552 (GClarkson 2011)
E_1(GPa)	158.5	127.3
E_2(GPa)	9.0	9.2
G_{12}(GPa)	4.7	4.8
ν_{12}	0.316	0.302
X_T(MPa)	2501	1996
X_C(MPa)	− 1716	− 1398
Y_T(MPa)	64.1	63.9
Y_C(MPa)	−286	− 268
S(MPa)	91.2	91.6
Ply thickness (mm)	0.183	0.188

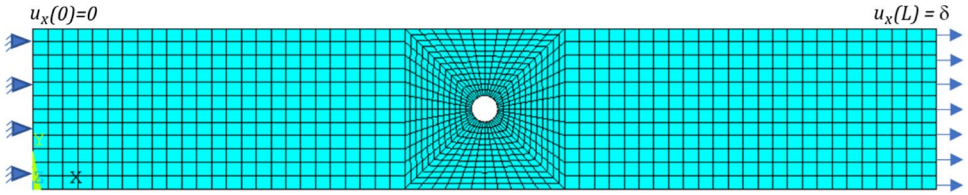

Fig. 5 The FEM model for the open-hole tension specimens tested by Marlett (Marlett et al. 2011) and Clarkson (2011)

Table 2 Comparison between the open-hole tension test results reported by Marlett (Marlett et al. 2011) and Clarkson (2011) and the numerical results obtained in this study regarding the ultimate failure stress of the specimens

Layup Sequence	Experimental Results (MPa)		Predictions of the Present Model (MPa)		Error %	
	AS4/8552 (Garnich and Akula 2009)	IM7/8552 (Marlett et al. 2011)	AS4/8552	IM7/8552	AS4/8552	IM7/8552
OHT1	328	407	325	396	− 1	− 3
OHT2	270	301	264	307	− 2	2
OHT3	473	597	433	542	− 8	− 9

Layup sequence is $[45/0/-45/90]_{2s}$ for OHT1, $[\pm 45/0/\pm 45/90/\pm 45/\pm 45]_s$ for OHT2, and $[0/45/0/90/0/-45/0/45/0/-45]_s$ for OHT3

of the results. The results are obtained using 1650 elements. Increasing the number of elements to 3300 makes less than a 2% difference but leads to a significant increase in the computational time. Because optimization requires a considerable number of iterations, the computational efficiency of the analyses is crucial. A convergence analysis is also performed regarding the number of increments in the displacement applied to the loaded edge of the plate. Trials with different numbers of sub-steps show that at least 200 substeps are required to ensure the accuracy of the results. Automatic load stepping is activated, which means that the finite element software calculates an optimum load step at the end of each substep based on the response of the structure to the applied loads. However, the minimum number of substeps is set to 200.

Table 2 compares the open-hole tension test results reported by Marlett (Marlett et al. 2011) and Clarkson (2011) and the numerical results obtained in this study regarding the ultimate failure stress of the specimens. The predictions for the quasi-isotropic specimens (OHT1) and the soft specimens (OHT2) are very close to the test results. For the hard specimens (OHT3), predictions are somewhat conservative. However, since the coefficient of variation of the test results was about 4%, the predictions can be considered acceptable. For the OHT3 specimens made of IM7/8552 material, the average ultimate stress in the tests was reported to be 597 MPa, while the minimum and maximum values were 545 MPa and 651 MPa, respectively (Marlett et al. 2011). Therefore, a prediction of 542 MPa, although on the conservative side, is within the experimental scatter.

Table 3 The material properties of the specimens tested by Schläpfer and Kress (Schläpfer and Kress 2014)

E_1(GPa)	130
E_2(GPa)	9
G_{12}(GPa)	4.25
ν_{12}	0.34
X_T(MPa)	2330
X_C(MPa)	− 1500
Y_T(MPa)	47
Y_C(MPa)	− 235
S(MPa)	79

3.2 Case 2

Schläpfer and Kress (Schläpfer and Kress 2014) conducted open-hole tension tests on specimens with $[0_2/45_2/-45_2]_s$ and $[0_2/45_2/-45_2]_{2s}$ layup sequences. The thickness of the plies was 0.125 mm. The dimensions of the specimens were 200 × 50 mm. The diameter of the hole at the center of the specimen was 20 mm. The material was carbon-fiber-reinforced epoxy with properties given in Table 3. To measure the first-ply failure load, they used two methods: digital image correlation (DIC) and acoustic emission (AE).

Figure 6 shows the area of the FE model meshed with SHELL181 elements and the boundary conditions. Following the same procedure, the first-ply and ultimate failure loads of the specimens are obtained. Table 4 compares the open-hole tension test results reported by Schläpfer and Kress (Schläpfer and Kress 2014) and the numerical results obtained in this study. For the thin specimen, the

Puck failure model predicts the first-ply failure load to be 11.33 kN, which is 13% higher than the test result. For the thick specimen, the prediction is 4% lower. Schläpfer and Kress (Schläpfer and Kress 2014) estimated almost the same values using the Tsai-Hill model. The ultimate failure loads predicted by the present model are quite satisfactory. For the thin plate, the predicted final failure load is 6% lower than the experimental result, while for the thick one, the predicted failure load is 1% higher than the experimental result.

Figure 7 shows the progression of damage in the thin specimen during the tension test (Schläpfer and Kress (Schläpfer and Kress 2014)) as predicted by the present model. Damage first initiates at the edge of the hole in the +45 and −45-degree plies at 0.60 mm applied displacement, corresponding to 11.33 kN resistive force. On the other hand, damage first occurs in the 0-degree plies at 21.27 kN (1.13 mm displacement). When the applied displacement is increased to 1.15 mm, the corresponding resistive force increases to 21.44 kN, then the plate becomes incapable of resisting a further increase in the load due to the progression of damage toward the edge of the plate. After that, the plate continues to deform and extend under lower loads. When the applied displacement becomes 1.26 mm, and the corresponding resistive force drops to 20.3 kN, then the damage in the +45 and −45 -degree plies extends to the edges of the plate, and a substantial portion of the fibers in the zero direction are also damaged as shown in Fig. 7.

4 Estimate of the ultimate failure load using first-ply-fiber failure anaysis

In composite structures, initial damage typically occurs due to matrix failure with few exceptions, like unidirectional laminates under uniaxial loading in the fiber direction. For this reason, the first-ply failure load can be considered as the load that causes initial matrix failure. Since composites behave as a linear elastic material up until the point of initial damage, the first-ply failure load can be

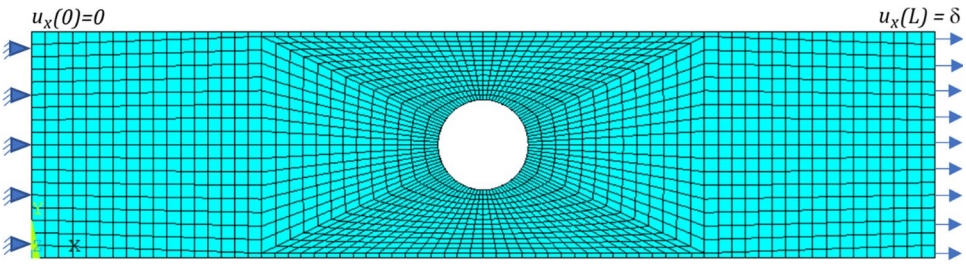

Fig. 6 The FEM model for the open-hole tension specimens tested by Schläpfer and Kress (Schläpfer and Kress 2014)

Table 4 Comparison between the open-hole tension test results reported by Schläpfer and Kress (Schläpfer and Kress 2014) and the numerical results obtained in this study regarding the first-ply failure load and ultimate failure load of the specimens

Layup Sequence	First-ply failure load (kN)			Ultimate failure load (kN)		
	Test results	Predictions	error %	Test results	Predictions	error %
$[0_2/45_2/-45_2]_s$	10.01	11.33	13	22.79	21.44	− 6
$[0_2/45_2/-45_2]_{2s}$	23.70	22.65	− 4	42.78	43.02	1

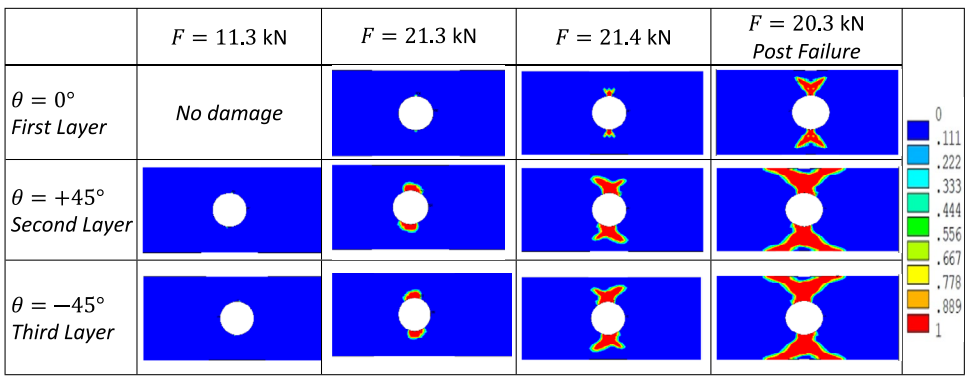

Fig. 7 The progression of damage in the thin specimen (Schläpfer and Kress (Schläpfer and Kress 2014)) as predicted by the present model

easily determined by conducting a linear elastic structural analysis and employing a reliable failure theory. On the other hand, to determine the ultimate failure load, a progressive failure analysis (PFA) is needed, which requires much longer computational times to yield results. In this study, the above-described progressive failure analysis is used to maximize the ultimate failure load. However, it is usually computationally too expensive to be used in real industrial applications where more complex and larger structures are involved. Considering this drawback, this study also investigates the effectiveness of using the first-ply failure load causing initial fiber damage instead of the ultimate failure load in optimizing local reinforcements.

The load-carrying capacity of composite materials is primarily due to the fibers. Failure of some fibers causes a redistribution of the load within the composite part, leading to increased stress in the undamaged fibers. This can even trigger further fiber failures. As the load is increased, the fibers suffer more damage, resulting in a degradation in stiffness. For this reason, the remaining strength can be assumed to be small after the initiation of fiber damage. Figure 2 shows a typical load–displacement diagram of a tension test specimen with an open-hole. While the load causing initial matrix damage, which is 21.6 kN, is a small fraction of the ultimate failure load of 44.1 kN, the initial fiber failure load of 39.7 kN, is very close to the ultimate load. Accordingly, the reinforcement designs optimized to maximize the load causing initial fiber damage can be expected to be optimized also for maximum ultimate strength.

Considering that the overall stiffness of composite structures is hardly affected by matrix damage, the first-ply fiber failure load is determined via a linear elastic structural analysis, neglecting prior matrix damage. Since no material degradation is assumed prior to the initial fiber damage, the computational burden in obtaining the first-ply fiber failure load is the same as that of the first-ply matrix failure load.

5 Design optimization methodology

The goal of optimization is to determine the most effective configuration out of a multitude of potential configurations based on a predetermined performance criterion. Solution of a design optimization problem involves the following steps: Formulating the objective function to be used as a measure of performance, formulating the constraint functions to be used to eliminate unacceptable configurations, selecting the optimization variables, which influence the objective and/or constraint functions, and choosing a suitable search algorithm.

5.1 Objective function

In order to solve an optimization problem, an objective function must be defined as a benchmark for evaluating the effectiveness of a design. The goal of this study is to maximize the first-ply as well as ultimate strength with minimum use of material. Accordingly, a multi-objective function, f, is defined as follows

$$f = \alpha_1 \frac{W}{W_b} + \alpha_2 \frac{F_{FPFb}}{F_{FPF}} + \alpha_3 \frac{F_{ultB}}{F_{ult}}, \tag{9}$$

where W is the weight of the plate reinforced with additional layers; W_b is the weight of the unreinforced base plate; F_{FPF} and F_{ult} are the first-ply and ultimate failure loads of the reinforced plate, respectively; F_{FPFb} and F_{ultB} are the corresponding values for the unreinforced base plate. The weighting coefficients, α_1,α_2, and α_3, reflect the designer's relative priorities for the individual terms. Given the higher priority on maximizing the ultimate strength, these coefficients are set to 0.3, 0.25, and 0.45 respectively. The selection of these weights in a multi-objective function influences the distribution of optimal solutions, following the principles of Pareto optimality. As discussed by Marler and Arora (2010), varying weight preferences shape the Pareto front, impacting both the final objective function values and the optimal values of the optimization variables. This sensitivity highlights the role of these coefficients in determining outcomes. Furthermore, normalizing the weight of the reinforced laminate and its first and last-ply failure loads with those of the unreinforced base laminate, ensures comparability between terms and avoids unit discrepancies.

5.2 Optimization variables and constraints

The choice of optimization variables heavily impacts the effectiveness of an optimization procedure. The parameters that have considerable influence on the objective function or the constraint functions should be selected as optimization variables. In this study, the fiber orientation angles, θ_i, and the sizes of the additional layers are selected as optimization variables.

The thickness of the layers may also be taken as optimization variables. However, to avoid increasing the computational burden, the thickness of the reinforcing layers is not varied during the optimization process but its effect as a design parameter is investigated by repeating the optimization process for different numbers of plies and thus obtaining the optimum reinforcement designs for different thicknesses. Similarly, the material of the reinforcements is also considered as a design parameter, not as an optimization variable. One may repeat the optimization process for different materials to obtain alternative optimum designs; however, in this

study, the material of the additional layers is taken the same as the material of the base plate.

As a constraint on the values of the optimization variables, the fiber orientation angles, θ_i, take values between −90° and +90°. Actually, this range covers all the possible fiber orientations. When a unidirectional loading in the 0° direction is considered, the optimum fiber orientation may not be close 90°. A large search domain including obviously nonoptimal regions unnecessarily increases the computational time. For this reason, the lower and upper limits on the angles are chosen as −60° and +60°.

As another constraint, upper and lower limits should be imposed on the sizes of the additional layers. First of all, if the base plate has an edge near the hole, the additional layers may not extend beyond the edge. Then, an upper limit should be set to avoid such cases. Considering that notches have a local effect and the stress state is hardly affected away from a notch, an upper limit should be imposed to prevent the reinforcements extend to far distances, which would unnecessarily increase the computational burden. There should be lower limits on the size of the reinforcing layers considering manufacturing constraints.

5.3 Search algorithm: the modified simulated annealing

In optimum structural design problems, typically, numerous local minima exist. Using a local search algorithm usually results in the optimization process converging to a local minimum close to the starting point. To find the best design in the solution domain, which is the globally optimal design, a reliable global search algorithm like the simulated annealing algorithm should be used.

Simulated annealing is a process inspired by physical annealing, where a group of atoms initially having high mobility at a high temperature, when slowly cooled down, attain the lowest-energy crystal state through random movements. Similarly, in simulated annealing, the best configuration is obtained by randomly changing design variables and thus randomly generating new configurations.

The optimization procedure uses a variant of the simulated annealing (SA) algorithm proposed before in references (Kayikci and Sonmez 2012; Akbulut and Sonmez 2011), with some improvements introduced in this study. Unlike the original SA algorithm (Kirkpatrick et al., 1983), which searches only the neighborhood of a single point, the modified SA algorithm keeps a set of current configurations like some other variants of SA (Ali et al., 2002), thus searches all their neighborhoods. This feature is similar to genetic algorithms, as they also retain a population of current configurations. The number of current configurations, N, is taken as

$$N = 9n, \tag{10}$$

where n is the number of the optimization variables. Optimization becomes more challenging when more variables are involved. This requires a larger population of current configurations to ensure that the algorithm's reliability remains high. The optimization process starts with a random generation of initial current configurations within the design domain. This is achieved by assigning random values to the optimization variables without violating the constraints. After that, the objective function values of the current configurations are calculated, and then they are ordered from the lowest to the highest. The first configuration, with the lowest objective function value, is the best, whereas the last one is the worst.

In each iteration, one of the current configurations is randomly selected. Then, a random configuration is generated in the neighborhood of the chosen current configuration by introducing random changes in its design using the following equations:

$$\begin{aligned} w' &= w + r_w \Delta w_{\max} \\ \ell' &= \ell + r_\ell \Delta \ell_{\max} \\ \theta_i' &= \theta_i + r_\theta \Delta \theta_{\max}, i = 1 \ldots n, \end{aligned} \tag{11}$$

where w and ℓ are the width and the length of the reinforcing layer in the chosen current configuration; θ_i is the fiber orientation angle of the ith layer, n is the total number of layers in the reinforcement; r_w, r_ℓ, and r_θ are random numbers generated between -1 and + 1; Δw_{max}, $\Delta \ell_{max}$, and $\Delta \theta_{max}$ are the maximum variations for the respective optimization variables. A new random configuration for the reinforcing layers is obtained by adding the random variations $r_w \Delta w_{max}$, $r_\ell \Delta \ell_{\max}$, and $r_\theta \Delta \theta_{max}$ to w, ℓ, and θ_i. If a constraint limit for an optimization variable is violated, this process is repeated.

Once a new random configuration is generated, its firstply and ultimate failure strengths are calculated by carrying out an FE analysis. Its objective function value is then calculated using Eq. (9). To determine whether the new configuration should be rejected or accepted as a new current configuration, its acceptability, A_t, is evaluated using the following equation similar to the original SA algorithm (Kirkpatrick et al., 1983),:

$$A_n = \begin{cases} 1 & \text{if } f_n \le f_w \\ \exp\left(-(f_n - f_w)/T_k\right) & \text{if } f_n > f_w \end{cases}, \tag{12}$$

where f_n is the objective function value of the new configuration; f_w is the objective function value of the current configuration on the $(7n + 1)^{th}$ place, which is one of the worse configurations; T_k is the control parameter for the kth Markow chain; in other words, inner loop. A_n is compared with a random number, P_r, between 0.0 and 1.0; if it is larger than P_r, it is accepted, if not rejected. If the new

configuration is better than the current configuration on the $(7n+1)^{th}$ place, meaning its objective function value is lower, then it is always accepted, as indicated in Eq. (12). If the new configuration is worse than the configuration ranked $(7n+1)$, it may still be accepted with a probability depending on the value of the control parameter, T_k. As implied in Eq. (12), the acceptability of a new configuration, A_n, is high at high values of the control parameter, T_k. It decreases as T_k is decreased during the optimization process, and towards the end, worse configurations are almost never accepted.

T_k controls the convergence of the optimization process in a way similar to how temperature controls micro-structural changes in the material during physical annealing. At the beginning of the optimization process, a high initial value should be used for T_k such that the acceptability, A_n, will be close to 1.0. Thus, almost all newly generated configurations are accepted. In this way, a large solution domain is searched. This is similar to the melting stage in the physical annealing process, where atoms can freely form any configuration. The initial value of the control parameter, T_0, is determined after randomly generating $9n$ initial current configurations within the solution domain. To ensure a high probability of acceptance of new configurations, T_0 should have a value such that even if a newly generated configuration has an objective function value equal to the worst initial current configuration, the probability of acceptance will be 0.99. Then, from Eq. (12), $A_n = 0.99 = \exp\left(-\left(f_{worst} - f_w\right)/T_0\right)$. Simplifying, one obtains

$$T_0 = -\frac{f_{worst} - f_w}{\ln(0.99)} \tag{13}$$

After carrying out a certain number of iterations in the inner loop called Markow chain, the value of T_k is decreased, and a new inner loop begins. This decrease in T_k should be gradual to allow for a thorough search of the solution domain without getting trapped in a local minimum. In a similar manner, if metals are slowly cooled down, thus allowing time for temperature-driven micro-structural changes to occur, then in the end, a crystal structure, which has the lowest-energy state, can be obtained. Fast cooling, on the other hand, results in a high-energy amorph structure. In SA, during the latter stages of optimization, T_k should be set to such low values that a new configuration worse than the current ones is rarely accepted. This is called the freezing stage, where atom arrangements are stable. The value of T_k in the kth inner loop is calculated as

$$T_k = \alpha_k T_{k-1}, \tag{14}$$

where T_{k-1} is the value of the control parameter in the previous inner loop, α_k is the reduction factor.

If a new configuration is accepted, it replaces a current configuration randomly selected among the $2n$ worst configurations, ranked between $7n+1$ and $9n$. After that, the current configurations are reordered, and the next iteration is started. Therefore, the first $7n$ configurations always remain in the current set unless a better configuration is found. The last $2n$ configurations, however, may be replaced with a configuration having a higher objective function value. At the initial phases of the optimization process, almost any configuration is accepted because T_k, thus acceptability, A_l, is high. Consequently, the worst $2n$ configurations are dispersed all around the solution domain. Since the new configurations are randomly generated around the current configurations including the worst configurations, the solution domain is thoroughly searched. In later stages, when T_k is reduced, the acceptability of new configurations having a higher objective function value decreases. As a result, the current configurations start to cluster around local minimums.

To ensure a comprehensive search of the solution domain in the early stages of optimization, new configurations should be generated by introducing large variations to the chosen current configuration. This can be achieved by setting large initial values for the maximum variations of the optimization variables, Δw_{max}, $\Delta \ell_{max}$ and $\Delta\theta_{max}$, in Eq. (11). In this study, one-fourth of the difference between the upper and lower limits on the optimization variables is taken as the initial maximum variation as

$$\begin{aligned} \Delta w_{imax} &= \left(w_u - w_l\right)/4 \\ \Delta \ell_{imax} &= \left(\ell_u - \ell_l\right)/4 \\ \Delta\theta_{imax} &= \left(\theta_u - \theta_l\right)/4 \end{aligned} \tag{15}$$

where w_u, ℓ_u, θ_u and w_l, ℓ_l, θ_l are the upper and the lower limits on the width, length, and fiber angle of the additional layers, respectively. Using such large initial values for the maximum variations, the algorithm can search a large neighborhood of the selected current configuration. In the later stages of the optimization, their values are reduced to facilitate convergence to the minimum. Otherwise, if the algorithm continues to use large variations, the likelihood of finding better configurations would become increasingly rare, and much longer times are required for convergence. The reduction scheme is based on the number of new good configurations found in an inner loop. Considering that $9n$ current configurations are ordered from the best to the worst, if the number of changes in the first $7n$ configurations is less than 10% of the total number of iterations in an inner loop, the values of Δw_{max}, $\Delta \ell_{max}$ and $\Delta\theta_{max}$ are decreased by 5% to restrict the search to a smaller domain and thus increase the likelihood of finding improved designs. In the final stages of optimization, the values of the maximum variations become so small that only the close neighborhood of the current configurations is searched; thereby the optimal point can be determined precisely. This procedure bears similarities with the physical annealing process, where the

mobility of the atoms depends on temperature. At elevated temperatures, atoms are in a state of disorderly motion, having mobility reaching such levels that they can move great distances. As the material cools down, the movements of the atoms slow down; as a result, they can form arrangements only on a small-scale. In a similar manner, the search process in SA is controlled by the maximum variations, Δw_{max}, $\Delta \ell_{max}$ and $\Delta\theta_{max}$, since they control the scale of variations in the current configurations.

In another respect, the maximum variations, Δw_{max}, $\Delta \ell_{max}$, and $\Delta\theta_{max}$, have a role in the optimization, much like temperature in physical annealing. The temperature must be slowly decreased to allow time-dependent microstructural changes to occur and thus to reach equilibrium. In simulated annealing, iterations should be continued in an inner loop until the likelihood of improvement becomes low, then an equilibrium state similar to physical annealing can be assumed to have been attained. When improvements in the first $7n$ current configurations become scarce in an inner loop, this indicates that further improvements are not likely with the current values of the maximum variations. The number of improvements in an inner loop is a better indication of equilibrium since it gives a precise measure. For this reason, instead of implementing the temperature reduction scheme of the original SA algorithm, the value of the control parameter is reduced depending on the reduction in the maximum variation. The value of the reduction factor, α_k in Eq. (14), is evaluated as

$$\alpha_k = \begin{cases} \alpha_{\min} & if\ L_a^k/L^k > \Delta\theta_{\max}/\Delta\theta_{i\max} \\ \alpha_{\max} & else \end{cases}, \tag{16}$$

where L^k is the number of new configurations tried in the kth inner loop, and L_a^k is the number of accepted configurations. Accordingly, L_a^k/L^k ratio is a measure of overall acceptability in an inner loop. $\Delta\theta_{imax}$ is the initial maximum variation in the fiber angles, $\Delta\theta_{max}$ is its current value. Note that $\Delta\theta_{max}/\Delta\theta_{imax}$ ratio is the same for all variables, which means $\Delta w_{max}/\Delta w_{imax} = \Delta\ell_{max}/\Delta\ell_{imax} = \Delta\theta_{max}/\Delta\theta_{imax}$. α_{max} and α_{min} are chosen to be 0.999 and 0.8. As long as the acceptance ratio, L_a^k/L^k, is larger than $\Delta\theta_{max}/\Delta\theta_{imax}$ ratio, the control parameter is reduced at a higher rate by multiplying with α_{min}. At start, $\Delta\theta_{max} = \Delta\theta_{imax}$, then this ratio is equal to one. According to Eqs. (12) and (13), the initial value of the control parameter, T_0, is high enough to accept nearly all new configurations. Then, during the initial stages of the optimization, L_a^k/L^k ratio is also close to 1.0. When the number of improvements in the current best 7n configurations becomes small,$\Delta\theta_{max}$ is reduced so that a smaller neighborhood of the current points is searched. With reduced $\Delta\theta_{max}/\Delta\theta_{imax}$, the temperature parameter is reduced at a higher rate, resulting in the reduction in the acceptance ratio, L_a^k/L^k. When $\Delta\theta_{max}$ approaches zero at the end of the optimization process, the temperature parameter also approaches zero. The acceptance probability of a new configuration with a higher objective function value, A_n, then becomes nearly zero as Eq. (12) suggests.

L^k, or the number of new configurations tried in the kth inner loop is another factor controlling convergence. To ensure that the neighborhoods of the current configurations are sufficiently searched, a sufficient number of iterations should be carried out at a given value of the control parameter, T_k.

$$L^k = round\{3n[1 + 2(\Delta w_{\max}/\Delta w_{i\max})]\} \tag{17}$$

where n is the number of the optimization variables, $\Delta w_{max}/\Delta w_{imax}$ is ratio of the maximum variation for an optimization variable to its initial value. With a larger the number of optimization variables, n, the optimization problem becomes more complex and difficult to solve. For this reason, the number of iterations in an inner loop should be higher with a higher number of optimization variables. Since L^k is, by definition, an integer number, the value of the expression on the right-hand side of Eq. (17) is rounded to the nearest integer. At the start, which means $k = 1$, Δw_{max} is equal to Δw_{imax}, then $L^k = 9n$. In the later stages of the optimization process, Δw_{max} is reduced whenever the number of improvements in the first $7n$ current configuration is less than 10% of L^k. Towards the end of the optimization process, Δw_{max} will become a small fraction of Δw_{imax}, and then L^k will become close to $3n$. The reason for this reduction in L^k during optimization is that in the early stages of optimization, many improved configurations are found, and many worse configurations are accepted due to high values of the control parameter, T_k. Thus, more trials are needed to search the neighborhood of the newly found current configurations. On the other hand, in the later stages of optimizations, changes in the current configurations become rare, and then extended search becomes unnecessary.

Iterations are continued according to the above-described procedure until the difference between the objective function values of the best and the worst current configurations becomes minimal.

Besides being computationally expensive, the drawback of the global search algorithms is that they contain many parameters that need to be tuned for the specific problem at hand; otherwise, the search may result in a suboptimal solution or become computationally very inefficient. Finding proper values for the parameters, on the other hand, requires time-consuming numerical experimentations. For this reason, their implementation is cumbersome. In contrast, by just providing an initial guess, the deterministic local search algorithms can proceed to search a local optimum point. To implement the original simulated annealing, besides the initial point, many other parameter values need to be provided, like initial value of the temperature parameter, initial

maximum variation, temperature reduction scheme, and the length of the inner loop. On the other hand, to implement the modified simulated annealing algorithm proposed in this study, one only needs to define the search domain by specifying the upper and lower limits of the optimization variables. The initial value of the control parameter, T_0, is determined using Eq. (13). Once the solution domain is specified, the initial maximum variations, Δw_{max}, $\Delta \ell_{max}$, and $\Delta \theta_{max}$ are calculated using Eq. (15). The maximum variations are decreased by 5% whenever the number of improvements in the first $7n$ current configurations in an inner loop is less than 10% of the total number of iterations in that loop as mentioned above. The reduction in the value of the control parameter, T_k, is made dependent on the maximum variations through Eq. (16). The number of new configurations generated in an inner loop, L^k, is determined using Eq. (17). Therefore, a user needs to specify only the upper and lower bounds of the optimization variables to implement the modified simulated annealing algorithm. For this reason, its application to new problems is much easier compared to the original SA.

6 Results and discussion

The procedure for optimizing the design of local reinforcements, as explained above, is applied to maximize the first-ply and ultimate strengths of open-hole tension test specimens. The geometry (Fig. 6) and the material properties are taken the same as those of the specimens tested by Schläpfer and Kress (Schläpfer and Kress 2014). The material properties of the carbon-reinforced epoxy are given in Table 3. The layup sequence of the base plate is $[0_2/45_2/-45_2]_s$, and the thickness of the plies is 0.125 mm. The same boundary conditions and the same FE model are used for the structural analysis, but with the addition of the reinforcing layers.

First, the single rectangular reinforcement, depicted in Figs. 1(a) and 8, is considered. To optimize the reinforcement, its width and length, w and ℓ, and the fiber orientation angles, α and θ, are varied. The thickness is kept constant during optimization. However, considering the thickness as a design parameter, the optimum reinforcement designs are separately obtained for two different thicknesses with layup sequences $[\pm\theta/0_2/45_2/-45_2]_s$ and $[\pm\alpha/\pm\theta/0_2/45_2/-45_2]_s$ in the reinforced region. The layup sequence of the base plate is not varied. Because the load is applied in the 0 ° direction, fiber angles close to 90 ° are not expected to be optimal. Accordingly, the upper and lower limits on the fiber orientation angles are chosen as 60 ° and -60 °, respectively. Because of the manufacturing constraints, the angles take discrete values. A suitable increment for the fiber angles should be chosen depending on the manufacturing precision. In this study, the results are

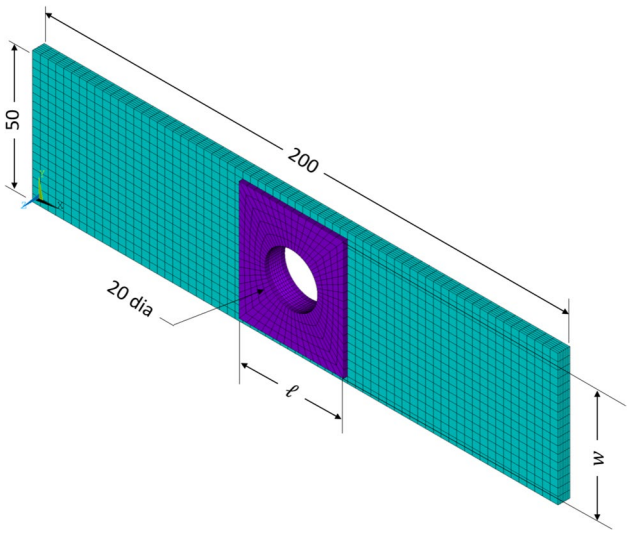

Fig. 8 Open-hole specimen model with a single rectangular reinforcement

obtained for 1 ° and 15 ° increments, which means the fiber angles are chosen from the following sets: (-60 °, -59 °, -58 °, …,58 °, 59 °, 60 °) or (-60 °, -45 °, -30 °, -15 °, 0 °, 15 °, 30 °, 45 °, 60 °). Considering that the width of the plate is 50 mm and the diameter of the circular hole is 20 mm, the upper and lower limits for the width of the reinforcement, w, are chosen as 48 mm and 28 mm, respectively. On the other hand, the upper and lower limits for the length of the reinforcement, ℓ, are chosen as 60 mm and 28 mm, respectively.

Another configuration for the reinforcement is the double rectangular layers placed at each side of the hole, as depicted in Figs. 1(b) and 9. For this type of reinforcement, the upper and lower limits for the width of the reinforcement, w, are taken as 4 mm and 14 mm, respectively. The upper and lower limits for the length, ℓ, are chosen as 90 mm and 28 mm, respectively. The layup sequence in the reinforced region is $[\pm\alpha/\pm\theta/0_2/45_2/-45_2]_s$.

Lastly, the reinforcement configuration with two rectangular overlapping layers, depicted in Figs. 1(c) and 10, is optimized. The optimization variables for this configuration are the fiber angles, α and θ, and the width and the length of each reinforcing layer, w_1, ℓ_1, w_2, and ℓ_2. The width and length of the larger reinforcing layer are constrained to satisfy $33\text{mm} \le w_1 \le 48\text{mm}$ and $33\text{mm} \le \ell_1 \le 60\text{mm}$. The width and length of the smaller reinforcing layer are constrained as $28\text{mm} \le w_2 \le w_1 - 5\text{mm}$ and $28\text{mm} \le \ell_2 \le \ell_1 - 5\text{mm}$. This means that the size of the upper reinforcing layer should be at least 5 mm smaller than that of the bottom reinforcing layer. This ensures a smoother transition between differently sized layers when the composite plate contains ply-drop-offs. In order to prevent delamination at ply-drop locations, a protective layer is typically used, as shown in

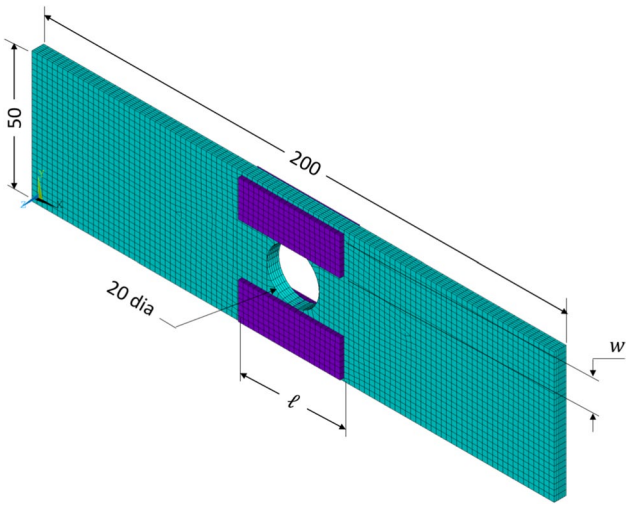

Fig. 9 Open-hole specimen model with double rectangular reinforcements at each side of the hole

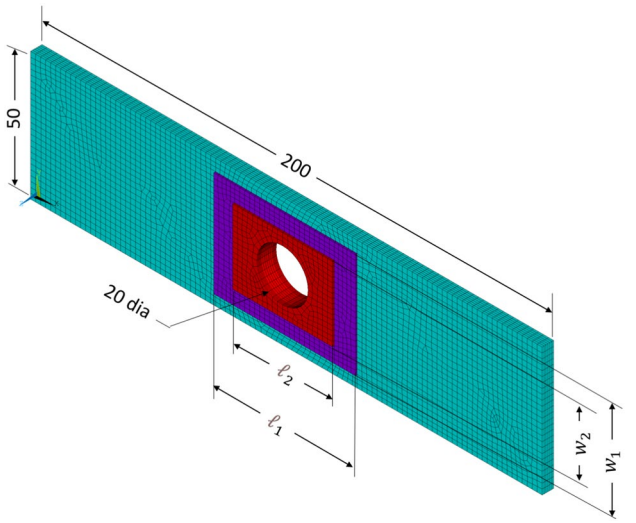

Fig. 10 Open-hole specimen model with two rectangular overlapping layers

Fig. 1(d). Because only membrane loads exist with no bending loads, 0 ° plies can be used as the protective layer with almost no change in the strength. Then, the suggested layup sequence for all three reinforcement configurations will be $[0_2/\pm\alpha/\pm\theta/45_2/-45_2]_s$.

Table 5 compares the strength levels of the unreinforced open-hole tension test specimen and the ones with optimal reinforcements. Optimization is performed for three different types of reinforcements. The first one is the single rectangular reinforcement (Figs. 1(a) and 8), optimized separately for two different thicknesses. For the thin one, the addition of a two-ply layer with 0 ° fiber orientation on each side of the plate results in 60.9% increase in the ultimate failure load

Table 5 Comparison between the strengths of the unreinforced open-hole tension test specimen and the ones with optimum reinforcements

Layup sequence	Reinforcement configuration	α	θ	Optimum values				First-ply strength (kN)	Ultimate strength (kN)	% increase in strength	% increase in weight
				w_1(mm)	ℓ_1(mm)	w_2(mm)	ℓ_2(mm)				
$[0_2/45_2/-45_2]_s$	No reinforcement	–	–	–	–	–	–	11.33	21.44	–	–
$[0_2/45_2/-45_2]_{2s}$	No reinforcement	–	–	–	–	–	–	22.65	43.02	100.6	100
$[\pm\theta/0_2/45_2/-45_2]_s$	Single (thin)	–	0	48.00	47.94	–	–	17.53	34.50	60.9	6.8
$[\pm\alpha/\pm\theta/0_2/45_2/-45_2]_s$	Single (thick)	2	1	47.99	47.80	–	–	22.37	49.19	129.4	13.6
$[\pm\alpha/\pm\theta/0_2/45_2/-45_2]_s$	Double at the sides	7	7	13.99	83.95	–	–	26.16	54.45	154.0	16.2
$[\pm\alpha/\pm\theta/0_2/45_2/-45_2]_s$	Two overlapping	1	0	47.98	50.44	42.93	36.59	22.13	49.16	129.3	11.6

The results for three different reinforcement types are presented: Single rectangular reinforcement (Figs. 1(a) and 8) with two different thicknesses, double rectangular layers placed at each side of the hole (Figs. 1(b) and 9), two rectangular overlapping layers (Figs. 1(c) and 10)

with only 6.8% increase in weight compared to the base plate with $[0_2/45_2/-45_2]_s$ layup sequence. With the addition of reinforcement with $[\pm 2/0_2]$ layup sequence, the final failure load increases by 129.4% with 13.6% increase in material use. On the other hand, the optimized double reinforcements placed at each side of the hole (Figs. 1(b) and 9) proved to be the most effective type of reinforcement in increasing the ultimate strength of the plate. 154% increase can be achieved in the ultimate failure load with only 16.2% increase in weight. If two overlapping reinforcements (Figs. 1(c) and 10) are optimized, the strength can be increased by 129.3% with 11.6% increase in the material used. All the reinforcement configurations proposed in this study are very effective in significantly improving the ultimate failure strength of the composite plates with a cutout under uniaxial tension load. As for the first-ply failure loads, the increase is 97.3% for the single reinforcement, 130.9% for the double reinforcements at the sides of the hole, and 95.2% for the overlapping reinforcements. Schläpfer and Kress (Schläpfer and Kress 2014) optimized local reinforcements to maximize the first-ply strength of the same base plate and achieved 100% increase (22.27 kN). Although it was not the direct objective of that study, the test results indicated 63.3% improvement in the ultimate failure strength. In this study, a similar improvement is obtained in the first-ply strength, but a significantly larger improvement is achieved in the ultimate strength. This demonstrates the importance of considering the ultimate failure strength in the design optimization of composite materials.

Figure 11 illustrates the change in first-ply and final failure loads as well as the mass of the best configuration through iterations for the double reinforcement design. The initial trial configuration exhibited a first-ply failure strength of 21.7 kN and a final-ply failure strength of 47.0 kN, with dimensions $\ell = 63$ mm and $w = 9$ mm and fiber orientations $[\pm\alpha/\pm\theta] = [\pm 14, /\pm 14]$. Through iterations, the dimensions and fiber orientations are tuned to make more effective use of the reinforcement. Ultimately, these adjustments led to the values given in Table 5.

Table 6 presents the optimal reinforcement designs obtained using the load causing initial fiber damage instead of the ultimate failure load, F_{ult}, in Eq. (9). The failure loads are determined directly based on the results of a linear elastic structural analysis without the need for a progressive failure analysis (PFA). The optimizations are conducted using the linear elastic analysis, but values of the first-ply fiber failure strength and the ultimate failure strength presented in Table 6 are obtained by carrying out a progressive failure analysis of the optimally reinforced plates.

A comparison of Table 5 and Table 6 shows that the strengths of the optimal reinforced plates using the first-ply fiber failure load are very close to those optimized using PFA. Although the results obtained using PFA are better, for practical engineering design problems, this alternative computationally much more efficient method can be used.

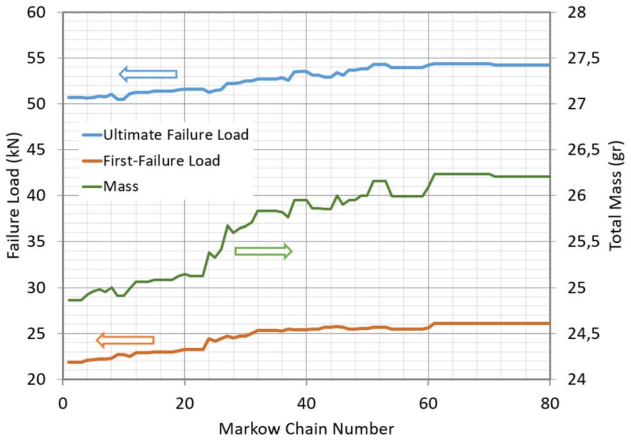

Fig. 11 The change in first-ply and final failure loads as well as the mass of the best configuration through iterations for the double reinforcement design

7 Conclusions

This study introduces a methodology to maximize the first-ply and ultimate strengths of composite plates with a cutout by optimizing local reinforcements in the form of additional rectangular layers. The ultimate strength is computed using a finite element method and implementing a progressive damage model based on the Puck failure criterion. The accuracy of the model predictions is verified by comparing them with open-hole tension test results. The progressive failure model proves effective in predicting the open-hole tension (OHT) ultimate failure strengths of carbon-fiber composites with various stacking sequences. The optimal reinforcement designs are determined using a modified simulated annealing algorithm. With the improvements introduced in this study, the simulated annealing algorithm is made more efficient and easier to apply. By providing only the upper and lower bounds of the variables, the algorithm can find the globally optimal point.

The proposed methodology is applied to an open-hole tension test specimen. Three different reinforcement configurations are tried, and they are found to be very effective in improving the first-ply and ultimate failure strengths. The improvements achieved using the optimal reinforcements are 95–130% in the first-ply failure strength and 130–155% in the ultimate failure strength with just a 12–16% increase in material use. The optimization algorithm identified the double rectangular reinforcements at each side of the hole with $[\pm 7/\pm 7]$ stacking sequence as the optimal reinforcement design, resulting in a 154%

Table 6 The optimum reinforcement designs obtained using the first-ply fiber failure load instead of the ultimate failure load, F_{ult}, in Eq. (9)

Reinforcement configuration	α	θ	Optimum values				Strength			% increase in		
			w_1(mm)	ℓ_1(mm)	w_2(mm)	ℓ_2(mm)	First-ply matrix (kN)	First-ply fiber (kN)	Ultimate (kN)	First-ply strength	Ultimate strength	weight
Single (thick)	0	0	47.99	47.51	–	–	22.07	48.89	48.89	94.6	128.0	13.5
Double at the sides	1	1	13.96	76.25	–	–	24.87	52.91	53.02	119.3	147.3	14.7
Two overlapping	1	5	47.87	47.96	42.72	36.16	21.83	48.13	48.15	92.5	124.6	10.8

increase in the ultimate failure load and a 131% increase in the first-ply load while adding only 16% to the weight of the unreinforced structure. One may conjecture that this fiber orientation optimizes the load distribution by altering the load path, improving the structural response in unreinforced regions. The results indicate that the optimal patch width nearly spans the entire plate width for both single and overlapping patches, while the optimal patch length is approximately equal to its width. Additionally, the optimal fiber orientation is between 0° and $\pm 2°$, aligning with the loading direction to maximize performance. The optimum double reinforcement also covers nearly the entire width of the plate, while its length is about 1.5 times its width.

Considering that use of a progressive failure analysis in the design optimization of composite parts is computationally inefficient for typical industrial applications, the applicability of maximizing the load that initiates fiber damage is investigated. The results show that maximizing the first-ply fiber failure load indirectly maximizes the ultimate failure load. Since the load causing initial fiber damage can be determined using a linear elastic structure analysis, this alternative method is computationally far more efficient.

The full potential of the design methodology proposed in this study should be further investigated, considering hybrid composite laminates, different types of loads and notch geometries. Then, the method can be applied to aircraft doors and windows, doorways, access ports, and other structural regions with stress concentrations, where localized reinforcement can enhance performance without significant weight increase.

Author contributions Sinan Kaya: Conceptualization, Methodology, Software, Validation, Formal analysis, Investigation, Writing—Original Draft, Visualization, Fazil O. Sonmez: Conceptualization, Methodology, Software, Validation, Formal analysis, Investigation, Resources, Writing—Original Draft, Writing—Review & Editing, Visualization, Supervision, Project administration, Funding acquisition.

Funding Open access funding provided by the Scientific and Technological Research Council of Türkiye (TÜBİTAK). This study is supported by Bogazici University Research Fund with grant number 18A06P1.

Declarations

Conflict of interest The authors state that there is no potential conflict of interest.

Replication of results The information provided in this paper is sufficient to replicate the results of this study. The codes will be provided by the corresponding author upon request.

Open Access This article is licensed under a Creative Commons Attribution 4.0 International License, which permits use, sharing, adaptation, distribution and reproduction in any medium or format, as long as you give appropriate credit to the original author(s) and the source,

provide a link to the Creative Commons licence, and indicate if changes were made. The images or other third party material in this article are included in the article's Creative Commons licence, unless indicated otherwise in a credit line to the material. If material is not included in the article's Creative Commons licence and your intended use is not permitted by statutory regulation or exceeds the permitted use, you will need to obtain permission directly from the copyright holder. To view a copy of this licence, visit http://creativecommons.org/licenses/by/4.0/.

References

Akbulut M, Sonmez FO (2011) Design optimization of laminated composites using a new variant of simulated annealing. Comput Struct 89(17–18):1712–1724

Ali MM, Törn A, Viitanen S (2002) A direct search variant of the simulated annealing algorithm for optimization involving continuous variables. Comput Oper Res 29(1):87–102

Almeida Jr JHS, Bittrich L, Spickenheuer A (2020) Improving the open-hole tension characteristics with variable-axial composite laminates: optimization, progressive damage modeling and experimental observations. Compos Sci Technol 185:107889

Alpay YO et al (2023) Failure behavior of laminated composite plates under anticlastic bending. J Reinf Plast Compos 42(7–8):281–299

Ambur DR, Jaunky N, Hilburger MW (2004) Progressive failure studies of stiffened panels subjected to shear loading. Compos Struct 65(2):129–142

Ambur DR et al (2004) Progressive failure analyses of compression-loaded composite curved panels with and without cutouts. Compos Struct 65(2):143–155

Arian Nik M et al (2022) Strength evaluation of continuous curvilinear variable stiffness panels with circular cutouts under biaxial normal loading and off-design conditions. Mech Adv Mater Struct 29(25):3860–3870

Barbero EJ (2010) Introduction to composite materials design. CRC Press, Boca Raton

Basu S, Waas AM, Ambur DR (2007) Prediction of progressive failure in multidirectional composite laminated panels. Int J Solids Struct 44(9):2648–2676

Camanho PP, Matthews F (1999) A progressive damage model for mechanically fastened joints in composite laminates. J Compos Mater 33(24):2248–2280

Catapano A, Desmorat B, Vannucci P (2015) Stiffness and strength optimization of the anisotropy distribution for laminated structures. J Optim Theory Appl 167(1):118–146

Chang F-K, Chang K-Y (1987) A progressive damage model for laminated composites containing stress concentrations. J Compos Mater 21(9):834–855

Chen J, Morozov E, Shankar K (2012) A combined elastoplastic damage model for progressive failure analysis of composite materials and structures. Compos Struct 94(12):3478–3489

Clarkson E (2011) Hexcel 8552 AS4 unidirectional prepreg qualification statistical analysis report. NCP-RP-2010–008 Rev D.

Deuschle HM, Puck A (2013) Application of the Puck failure theory for fibre-reinforced composites under three-dimensional stress: comparison with experimental results. J Compos Mater 47(6–7):827–846

Din IU et al (2018) Elastoplastic CDM model based on Puck's theory for the prediction of mechanical behavior of fiber reinforced polymer (FRP) composites. Compos Struct 201:291–302

Ferreira RT, Ashcroft IA (2020) Optimal orientation of fibre composites for strength based on Hashin's criteria optimality conditions. Struct Multidiscip Optim 61(5):2155–2176

Garnich MR, Akula VM (2009) Review of degradation models for progressive failure analysis of fiber reinforced polymer composites. Appl Mech Rev 62(1):10

Gotsis P, Chamis CC, Minnetyan L (1998) Prediction of composite laminate fracture: micromechanics and progressive fracture. Compos Sci Technol 58(7):1137–1149

Gotsis P, Chamis C, Minnetyan L (2004) Application of progressive fracture analysis for predicting failure envelopes and stress-strain behaviors of composite laminates: a comparison with experimental results. Failure criteria in fibre-reinforced-polymer composites. Elsevier, pp 703–725

Goyal VK et al (2004) Intralaminar and interlaminar progressive failure analyses of composite panels with circular cutouts. Compos Struct 64(1):91–105

Gummadi L, Palazotto A (1998) Progressive failure analysis of composite cylindrical shells considering large rotations. Compos B Eng 29(5):547–563

Günel M, Kayran A (2013) Non-linear progressive failure analysis of open-hole composite laminates under combined loading. J Sandwich Struct Mater 15(3):309–339

Hallett S et al (2009) An experimental and numerical investigation into the damage mechanisms in notched composites. Compos A Appl Sci Manuf 40(5):613–624

Hinton M, Kaddour AS, Soden PD (2004) Failure criteria in fibre reinforced polymer composites: the world-wide failure exercise. Elsevier, Amsterdam

Huang J, Haftka R (2005) Optimization of fiber orientations near a hole for increased load-carrying capacity of composite laminates. Struct Multidiscip Optim 30(5):335–341

Huang G, Wang H, Li G (2016) An efficient reanalysis assisted optimization for variable-stiffness composite design by using path functions. Compos Struct 153:409–420

Hyer MW, Lee H (1991) The use of curvilinear fiber format to improve buckling resistance of composite plates with central circular holes. Compos Struct 18(3):239–261

Irvine TB, Ginty CA (1986) Progressive fracture of fiber composites. J Compos Mater 20(2):166–184

Izzi MI, Catapano A, Montemurro M (2021) Strength and mass optimisation of variable-stiffness composites in the polar parameters space. Struct Multidiscip Optim 64(4):2045–2073

Joseph AP et al (2015) Progressive damage and failure prediction of open hole tension and open hole compression specimens. In: 56th AIAA/ASCE/AHS/ASC structures, structural dynamics, and materials conference.

Kayikci R, Sonmez FO (2012) Design of composite laminates for optimum frequency response. J Sound Vib 331(8):1759–1776

Khani A et al (2011) Design of variable stiffness panels for maximum strength using lamination parameters. Compos B Eng 42(3):546–552

Khani A et al (2017) Design, manufacturing and testing of a fibre steered panel with a large cut-out. Compos Struct 180:821–830

Kim Y, Davalos JF, Barbero EJ (1996) Progressive failure analysis of laminated composite beams. J Compos Mater 30(5):536–560

Kirkpatrick S, Gelatt CD Jr, Vecchi MP (1983) Optimization by simulated annealing. Science 220(4598):671–680

Knops M (2008) Analysis of failure in fiber polymer laminates: the theory of Alfred Puck. Springer Science & Business Media, Cham

Kong CW et al (1998) Postbuckling and failure of stiffened composite panels under axial compression. Compos Struct 42(1):13–21

Kweon J (1998) Post-failure analysis of composite cylindrical panels under compression. J Reinf Plast Compos 17(18):1665–1681

Lapczyk I, Hurtado JA (2007) Progressive damage modeling in fiber-reinforced materials. Compos A Appl Sci Manuf 38(11):2333–2341

Lee CS et al (2015) Initial and progressive failure analyses for composite laminates using Puck failure criterion and damage-coupled finite element method. Compos Struct 121:406–419
Le-Manh T, Lee J (2014) Stacking sequence optimization for maximum strengths of laminated composite plates using genetic algorithm and isogeometric analysis. Compos Struct 116:357–363
Liu K-S, Tsai SW (1998) A progressive quadratic failure criterion for a laminate. Compos Sci Technol 58(7):1023–1032
Liu X, Wang G (2007) Progressive failure analysis of bonded composite repairs. Compos Struct 81(3):331–340
Lopes CS, Gürdal Z, Camanho P (2010) Tailoring for strength of composite steered-fibre panels with cutouts. Compos A Appl Sci Manuf 41(12):1760–1767
Maimí P et al (2007a) A continuum damage model for composite laminates: Part II–computational implementation and validation. Mech Mater 39(10):909–919
Maimí P et al (2007b) A continuum damage model for composite laminates: part I-constitutive model. Mech Mater 39(10):897–908
Marler RT, Arora JS (2010) The weighted sum method for multi-objective optimization: new insights. Struct Multidiscip Optim 41:853–862
Marlett K, Ng Y, Tomblin J (2011) Hexcel 8552 IM7 unidirectional prepreg 190 gsm & 35% RC qualification material property data report. Nat Center Adv Mater Perform 11:1–238
Mathias JD, Balandraud X, Grediac M (2006) Applying a genetic algorithm to the optimization of composite patches. Comput Struct 84(12):823–834
Matsuzaki R et al (2021) Optimization of curvilinear fiber orientation of composite plates and its experimental validation. Compos Struct 255:112956
McCarthy CT, McCarthy MA, Lawlor V (2005) Progressive damage analysis of multi-bolt composite joints with variable bolt–hole clearances. Compos B Eng 36(4):290–305
Moure M et al (2015) Damage evolution in open-hole laminated composite plates subjected to in-plane loads. Compos Struct 133:1048–1057
Nikbakt S, Kamarian S, Shakeri M (2018) A review on optimization of composite structures Part I: laminated composites. Compos Struct 195:158–185
O'Higgins R et al (2004) Experimental and numerical study of the open-hole tensile strength of carbon/epoxy composites. Mech Compos Mater 40(4):269–278
Padhi G et al (1997) Progressive failure and ultimate collapse of laminated composite plates in bending. Compos Struct 40(3–4):277–291
Philippidis TP, Antoniou AE (2013) A progressive damage FEA model for glass/epoxy shell structures. J Compos Mater 47(5):623–637
Prusty BG (2005) Progressive failure analysis of laminated unstiffened and stiffened composite panels. J Reinf Plast Compos 24(6):633–642
Puck A, Mannigel M (2007) Physically based non-linear stress–strain relations for the inter- fibre fracture analysis of FRP laminates. Compos Sci Technol 67(9):1955–1964
Puck A, Schürmann H (2004) Failure analysis of FRP laminates by means of physically based phenomenological models. Failure criteria in fibre-reinforced-polymer composites. Elsevier, pp 832–876
Puck A, Kopp J, Knops M (2002) Guidelines for the determination of the parameters in Puck's action plane strength criterion. Compos Sci Technol 62(3):371–378
Riccio A et al (2017) Intra-laminar progressive failure analysis of composite laminates with a large notch damage. Eng Fail Anal 73:97–112
Ridha M et al (2014) Modelling complex progressive failure in notched composite laminates with varying sizes and stacking sequences. Compos A Appl Sci Manuf 58:16–23
Schläpfer B, Kress G (2014) Optimal design and testing of laminated light-weight composite structures with local reinforcements considering strength constraints part i: design. Compos A Appl Sci Manuf 61:268–278
Shroff S, Kassapoglou C (2015) Progressive failure modelling of impacted composite panels under compression. J Reinf Plast Compos 34(19):1603–1614
Sonmez FO (2017) Optimum design of composite structures: a literature survey (1969–2009). J Reinf Plast Compos 36(1):3–39
Soutis C, Fleck N, Smith P (1991) Failure prediction technique for compression loaded carbon fibre-epoxy laminate with open holes. J Compos Mater 25(11):1476–1498
Spottswood SM, Palazotto AN (2001) Progressive failure analysis of a composite shell. Compos Struct 53(1):117–131
Su Z et al (2015) Progressive damage modeling of open-hole composite laminates under compression. Compos Struct 122:507–517
Tan SC (1991) A progressive failure model for composite laminates containing openings. J Compos Mater 25(5):556–577
Tan SC, Perez J (1993) Progressive failure of laminated composites with a hole under compressive loading. J Reinf Plast Compos 12(10):1043–1057
Tanaka H et al (2021) Multi-objective optimization of weight and strength of laminated composites using gap-less and overlap-less variable thickness fiber placement. Compos Struct 276:114562
Xie D, Biggers SB Jr (2003) Postbuckling analysis with progressive damage modeling in tailored laminated plates and shells with a cutout. Compos Struct 59(2):199–216
Zehnder N, Ermanni P (2006) A methodology for the global optimization of laminated composite structures. Compos Struct 72(3):311–320
Zhang B, Zhao L (2012) Progressive damage and failure modeling in fiber-reinforced laminated composites containing a hole. Int J Damage Mech 21(6):893–911
Zhou S et al (2017) Progressive damage simulation of open-hole composite laminates under compression based on different failure criteria. J Compos Mater 51(9):1239–1251

Publisher's Note Springer Nature remains neutral with regard to jurisdictional claims in published maps and institutional affiliations.